Force-Generating Cross-Bridges during Ramp-Shaped Releases: Evidence for a New Structural State

A. Radocaj,[†] T. Weiss,[‡] W. I. Helsby,[§] B. Brenner,[†] and T. Kraft[†*]
[†]Department of Molecular and Cell Physiology, Hannover Medical School, Hannover, Germany; [‡]European Synchrotron Radiation Facility, Grenoble, France; and [§]Daresbury Laboratory, Daresbury, Warrington WA4 4AD, United Kingdom

ABSTRACT Mechanical and two-dimensional (2D) x-ray diffraction studies suggest that during isometric steady-state contraction, strongly bound cross-bridges mostly occupy early states in the power stroke, whereas rigor or rigor-like cross-bridges could not be detected. However, it remained unclear whether cross-bridges accumulate, at least transiently, in rigor or rigor-like states in response to rapid-length releases. We addressed this question using time-resolved recording of 2D x-ray diffraction patterns of permeabilized fibers from rabbit psoas muscles during isometric contraction and when small, ramp-shaped length-releases were applied to these fibers. This maneuver allows a transient accumulation of cross-bridges in states near the end of their power stroke. By lowering the temperature to 5 °C, force transients were slowed sufficiently to record diffraction patterns in several 2–4-ms time frames before and during such releases, using the RAPID detector (Refined ADC Per Input Detector) at beam line ID02 of the European Synchrotron Radiation Facility (Grenoble, France). The same sequence of frames was recorded in relaxation and rigor. Comparisons of 2D patterns recorded during isometric contraction, with patterns recorded at different [MgATPγS] and at 1 °C, showed that changes in intensity profiles along the first and sixth actin layer lines (ALL1 and ALL6, respectively) allowed for discernment of the formation of rigor or rigor-like cross-bridges. During ramp-shaped releases of activated fibers, intensity profiles along ALL1 and ALL6 did not reveal evidence for the accumulation of rigor-like cross-bridges. Instead, changes in the ALL6-profile suggest that during ramp-shaped releases, cross-bridges transiently accumulate in a structural state that, to our knowledge, was not previously seen, but that could well be a strongly bound state with the light-chain binding domain in a conformation between a near prepower-stroke (isometric) orientation and the orientation in rigor.

INTRODUCTION

It is generally accepted that muscle contraction is driven by a series of conformational changes of the actin-attached myosin head (cross-bridge). This series of conformational changes, the so-called ''power stroke,'' is coupled to the release of the ATP-hydrolysis products, phosphate and ADP, from the active site (1). Various approaches were used to characterize the structural changes of the actomyosin cross-bridge and their relationship to the ATPase cycle. Based on early x-ray fiber diffraction data (2), it was proposed that force generation in muscle occurs when actin-attached myosin heads reach a conformation like that seen in the absence of nucleotide (rigor) (3). Based on data from protein crystallography (4) and cryo-electron microscopy of actin filaments decorated with myosin head domains in the absence of nucleotide (5,6), this concept seemed to receive further support (5,7–9). According to this concept, late, rigor-like states of the power stroke were thought responsible for the generation of isometric force. Even the earliest x-ray diffraction studies of muscle during isometric contraction, however, failed to reveal features characteristic of rigor cross-bridges (10,11). More recent x-ray studies (12–18) were no more successful.

Based on mechanical studies of intact frog fibers, it was also proposed that isometric force is generated when cross-bridges, after an initial firm attachment, proceed to subsequent states of a power stroke (19). According to this concept, the rapid recovery of force after a stepwise length release was thought to result from additional cross-bridges proceeding from initial firm attachment to later states in the power stroke, i.e., the generation of isometric force and the rapid recovery of force in response to length releases were thought to result from the same basic molecular mechanism. According to this proposal, length releases, imposed on muscle fibers during isometric contraction, were expected to drive cross-bridges toward later states of their power stroke, whereas stretches would drive cross-bridges back to earlier states of the power stroke (19). Consequently, force transients during and after both stretches and releases should reveal signatures of redistribution among different states of the power stroke (19).

Mechanical studies of skinned muscle fibers from the rabbit, however, revealed that isometric force is most likely already generated when cross-bridges enter the early states of a power stroke (20,21). This conclusion was based on the observed asymmetry in force transients during ramp-shaped stretches versus ramp-shaped releases. During releases, cross-bridges redistributed toward later states of the power stroke, as previously proposed by Huxley and Simmons (19). During stretches imposed during an isometric steady state, however, there was no evidence for significant redistribution from later states back to earlier states in the power

Submitted July 25, 2008, and accepted for publication November 13, 2008.

*Correspondence: Kraft.Theresia@MH-Hannover.de

T. Weiss's present address is SSRL/SLAC, Stanford University, 2575 Sand Hill Road, MS69, Menlo Park, CA 94025-7015.

Editor: K. W. Ranatunga.

0006-3495/09/02/1430/17 $2.00

doi: 10.1016/j.bpj.2008.11.023

stroke (20). This was consistent with a concept in which isometric force is already generated when cross-bridges reach early, strong binding states of the power stroke, i.e., states before those that become occupied after quick tension recovery in response to a stepwise length release (20,21). We propose that force generation in the early states of a power stroke results from redocking of the light-chain binding domain, for example, when myosin heads proceed from nonstereospecific, weak actin binding to stereospecific and strong actin binding, whereas the light-chain binding domain remains near its prepower-stroke conformation. During isometric steady state, according to our concept, only a few cross-bridges are thought to occupy the later states in a power stroke. According to this concept, the occupancy of later states in a power stroke, e.g., with the light-chain binding domain near a postpower-stroke rigor-(like) conformation, would be expected to increase transiently, in response to stepwise or ramp-shaped length releases (21).

The concept that isometric force is generated by cross-bridges in early states of the power stroke is consistent with x-ray diffraction data (10–14,16) indicating no rigor-like features during isometric steady-state contraction. These studies, however, did not allow more detailed conclusions regarding whether the cross-bridge states occupied during an isometric steady-state contraction were at the beginning or nearer the end of a power stroke. Mechanical studies were interpreted to show that isometric force is already generated before the release of inorganic phosphate from the active site (22–25). These results are consistent with the concept that isometric force is generated in early states of the power stroke, although no conclusions were possible about structural features of the cross-bridges that generate isometric force. A concept essentially identical to ours (20,21) was proposed on the basis of experiments where x-ray diffraction and mechanical perturbations, imposed during isometric contraction and in rigor, were used (15). It was proposed that the strongly bound myosin head assumes a postpower-stroke, rigor-like conformation only after quick tension recovery in response to a stepwise length release imposed during isometric steady-state contraction. Isometric force, generated before the release, was thought to result from myosin heads in a conformation closer to the prepower-stroke conformation, with the lever arm tilted ~30° away from the rigor conformation (15). Ferenczi et al. (17) proposed a concept in which isometric force was again thought to be generated already at the transition from non-stereospecific to stereospecific binding of the myosin motor domain to actin, with additional force and additional movement generated by rotation of the lever arm, e.g., in response to stepwise length releases. This proposal was based on x-ray diffraction and T-jump experiments, combined with imposed stepwise length changes (17).

Although these concepts predicted that in response to stepwise or ramp-shaped releases, cross-bridges should, at least transiently, accumulate in states near the end of a power stroke, i.e., in rigor or-rigor like states structurally, it remained unclear whether this could be detected experimentally. We therefore recorded two-dimensional (2D) x-ray diffraction patterns with a high time resolution before and during ramp-shaped releases imposed after isometric force had reached steady state. We specifically aimed at time periods before and after the retardation in the decrease in active force during a ramp-shaped release. This retardation had been interpreted as a signature of regeneration of force upon redistribution of cross-bridges toward later states in a power stroke (20,21,26), equivalent to the rapid tension recovery in response to stepwise length changes (27). To allow sufficient time to place a time frame in the period before the retardation in the decrease in active force, the temperature was lowered to 5°C, to slow the redistribution of cross-bridges toward later states in the power stroke. We focused our analysis on the parts of diffraction patterns that are sensitive to an accumulation of rigor like cross-bridges, i.e., the first actin layer line (ALL1), the sixth actin layer line (ALL6), and the equatorial 1,1 and 1,0 reflections. The effects of rigor cross-bridges on these features were probed by lowering the concentration of MgATPγS, thus generating an increasing fraction of nucleotide-free rigor cross-bridges (16).

In diffraction patterns recorded during ramp-shaped releases, we were unable to detect changes toward features typical of cross-bridges in a rigor(-like) conformation, both on ALL1 and ALL6. Instead, patterns recorded after the pause in the tension decline during ramp-shaped releases exhibited a change in intensity profile along ALL6, indicating an accumulation of cross-bridges in a conformation different from both the conformation seen during isometric contraction and the rigor conformation. A preliminary account of this work was presented as an abstract (28).

MATERIALS AND METHODS

Single-fiber preparation, solutions, and length control

Single fibers were isolated from bundles of chemically skinned fibers of M. psoas of rabbits, as described previously (29–31). The entire procedure of mounting arrays of Triton-permeabilized single fibers for x-ray diffraction, and methods for reducing beam damage, were introduced elsewhere (16,32). For the experiments presented here, ~15 (for time-resolved experiments at the European Synchrotron Radiation Facility) or 30 (for recording patterns at the SRS or at HASYLAB) single fibers were mounted side-by-side in the muscle chamber of the x-ray setup. We used arrays of single fibers instead of natural fiber bundles, to minimize distances for the diffusion of substrate and products into and out of the fibers (32). In addition, to minimize temperature gradients and concentration gradients, especially in the small gap between the Kapton windows where the x-ray beams pass through, the solution in the experimental chamber was continuosly pumped up and down.

One end of the fiber array was attached to a linear motor (Scientific Instruments, Heidelberg, Germany), and the other to a strain gauge force transducer (Akers, Horten, Norway). Fiber length was adjusted by the linear motor via length-controlled feedback. It was set such that sarcomere length, measured by laser light diffraction using a 633-nm helium-neon laser, was

2.4 μm. To increase maximum exposure time, fibers were scanned up and down in the x-ray beam so that ~6 mm of fiber length were exposed to the x-rays. For recording diffraction patterns from activated fibers, the solution change from relaxing to activating solution, and back to relaxing solution, occurred via remote-controlled syringe pumps.

Solutions for relaxation (pCa 8), rigor, and maximum Ca^{2+} activation (pCa 4.5) were identical to those in our previous work (16,32). For comparison, patterns with different MgATPγS concentrations in the absence of MgATP were recorded, but on a separate set of fiber arrays. The constituents of these solutions were the same as described elsewhere (32,33). For the experiments described here, all MgATPγS solutions contained a Ca^{2+} concentration sufficient for maximal activation (pCa 4.5), to minimize differences in diffraction patterns originating from the effects of Ca^{2+} on regulatory proteins. All solutions with MgATPγS also contained 0.2 mM Ap_5A as myokinase inhibitor and 200 mM glucose, together with 0.5 units/mL of hexokinase to remove traces of MgATP. For the MgATPγS experiments, the temperature was reduced to 1 °C, to enhance the saturation of myosin heads with MgATPγS, such that nearly full saturation was achieved with 1 mM MgATPγS, even at the saturating Ca^{2+} concentrations (pCa 4.5) used in this study (33).

The experimental temperature for activation, relaxation, and rigor conditions was set at 5°C, to slow down the redistribution of cross-bridges among different intermediate states of the ATPase cycle during ramp-shaped releases, such that time frames of 2–4 ms could be placed before and after the delay in the force decline during ramp-shaped releases. At this temperature and at an ionic strength of 170 mM, we previously found isometric force to be 58 ± 20 kN/m^2 (mean ± SD, n = 10) and 37% ± 7% (mean ± SD, n = 8 fibers) of the isometric force at 20 °C, and ~1/3 of the force observed at 25–35°C, in agreement with other studies (34–37).

The ionic strength of all solutions here was adjusted to 80 mM by potassium propionate. This ionic strength was chosen to mimic, as closely as possible, intracellular ionic-strength conditions. Godt and Maughan showed that the main anion in the sarcoplasm of muscle fibers is phosphocreatine (as potassium salt), and that it is present at concentrations of 45–55 mM (38). When we compared equatorial intensities (including higher-order reflections) recorded in relaxing solution with 40 mM K_2 phosphocreatine with equatorial intensities observed in relaxing solutions but with ionic strength adjusted by K propionate, we found the best match of equatorial intensities when the ionic strength, adjusted by K propionate, was ~80 mM. We used 40 mM K_2 phosphocreatine as reference, to allow for contributions to ionic strength by other constituents (e.g., EGTA) in the reference relaxing solution that were not present in native muscle fibers. As a result, we have come to use a standard ionic strength of 80 mM (16,39). The apparently low "effective" ionic strength in the presence of 40 mM K_2 phosphocreatine most likely results from the limited dissociation (low activity coefficient) of K_2 phosphocreatine. At 80 mM ionic strength, adjusted by K propionate, we found isometric forces ~1.5 ± 0.2 times higher than at 170 mM ionic strength, and ~1.8-fold higher than at 200 mM ionic strength. Thus, isometric force under our experimental conditions, i.e., 5°C and ionic strength 80 mM (adjusted by K propionate), is 50–60% of the force seen at 25–35°C and at an ionic strength of 170–200 mM in our own controls and in other studies (34–37).

Time-resolved x-ray diffraction experiments at the European Synchrotron Radiation Facility

Two-dimensional, low-angle x-ray diffraction patterns of single-fiber arrays were collected at beam line ID02 of the European Synchrotron Radiation Facility (ESRF, Grenoble, France). This beam line provided an x-ray flux of up to 3 × 10^{13} photons s^{-1} at a 0.1-nm wavelength. The 2D diffraction patterns were recorded with the gas-filled Refined ADC Per Input Detector (RAPID) developed at the Synchrotron Radiation Source (SRS, Daresbury, Warrington, UK) (40,41). The RAPID detector was installed on a bypass parallel to the standard ID02 beam line, resulting in lower x-ray flux compared with a standard beam line. To maximize available flux, both undulators of ID02 were in use. The size of the active area of the detector was 200 mm × 200 mm, and the camera length was 6.2 m. With this camera length, only one quadrant of the diffraction patterns could be recorded, ranging from the equator to the sixth actin-based layer line (ALL6) at a reciprocal spacing of 1/5.9 nm^{-1}, whereas only smaller parts of adjacent quadrants were covered (see Fig. 2 *B*). Equatorial intensities were attenuated ~3.5-fold by a thin strip of lead, to minimize possible reduction in detector sensitivity because of dead-time effects in rows and columns with high local intensities at the equatorial 1,0 and 1,1 reflections.

The RAPID detector is a position-sensitive photon-counting device. This detector enabled us to record single "snapshots" of 2D diffraction patterns within time frames of 2–4 ms. Although the photon count in an individual snapshot is rather low (Fig. 1 *A*), the very low readout noise of a photon-counting device allowed us to add up a large number of individual snapshots. Thus, even in time windows as short as 2–4 ms, diffraction patterns can be obtained with sufficient intensity in the off-meridional actin-based and myosin-based layer lines (Fig. 1 *B*). The actual number of added snapshots was between 560–800, depending on the number of fiber arrays from which data were recorded and summed up. In test trials with a CCD detector, a similarly successful generation of 2D diffraction patterns by the accumulation of individually recorded snapshots was not possible, i.e., the weaker reflections and layer lines remained covered in noise. This outcome was presumably attributable to the high readout noise of this detector type. The duration of snapshots (2–4 ms) was dictated by the time course of the force response to ramp-shaped releases under our experimental conditions.

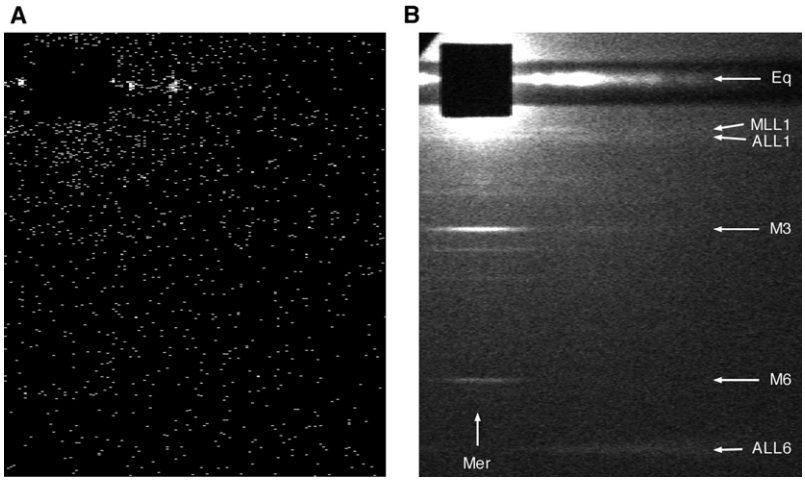

FIGURE 1 2D x-ray diffraction patterns recorded with RAPID detector at ESRF in Grenoble. (*A*) Single "snapshot" of 2-ms exposure shows signals of individual photons. Signals of individual photons are horizontal lines, four pixels in length, because fourfold binning and unbinning of frames in horizontal direction during data acquisition and data analysis, respectively, were inevitable (details in Materials and Methods). (*B*) 2D x-ray diffraction pattern recorded during isometric steady-state contraction in 3-ms time frame immediately before start of ramp-shaped release (time frame I; see Fig. 2 *A*). For this pattern, 800 snapshots, recorded within time frame I of 800 ramp-shaped releases collected from six single-fiber arrays, were added up. Resultant total accumulated exposure time was 2.4 s. MLL1, first myosin-based layer line; ALL1, first actin-based layer line; ALL6, sixth actin-based layer line; M3, first-order meridional reflection of myosin heads; M6, second-order meridional reflection of myosin heads; Mer, meridian; Eq, equator.

Experimental protocol

After a fiber array, mounted in the x-ray path, reached steady isometric force, it was subjected to repeated length changes (ramp-shaped releases; Fig. 2 *A*). In such ramp-shaped releases, fibers were allowed to shorten linearly with time, and were restretched to their original length after each such release. The amplitude of these ramp-shaped releases was 1.6–1.7% of the overall fiber length, i.e., equivalent to $\leq$20 nm of filament sliding, and with the retardation of tension decline taking place between $\leq$2–8 nm of filament sliding (Fig. 2 *A*, *bottom*). The ramp-shaped releases lasted for 20 ms, and were followed by a restretch to the original fiber length within 4 ms. These ramp-shaped length changes were repeated after a 0.3-s period of isometric contraction. The timing of releases is shown in Fig. 2 *A* (*middle*). After five such ramp-shaped release/restretch maneuvers, a period of nearly unloaded active shortening was allowed for 100 ms, followed by restretch to the original fiber length. After a waiting period during which isometric force redeveloped to its steady-state level, a new cycle of five ramp-shaped releases was initiated. Unloaded shortening with restretch to original length after five ramp-shaped releases was used to stabilize fiber structure, i.e., to avoid increasing disorder of sarcomeres that would have otherwise developed in the skinned fibers during longer periods of isometric force generation (29). For each fiber array, the complete cycle, consisting of isotonic shortening, restretch with redevelopment of force to the isometric steady-state, and five ramp-shaped length release/restretch maneuvers, was repeated 28 times (Fig. 2 *A*, *top*), except for one fiber array where the total protocol was terminated after 20 cycles because of a sudden rapid force decay, presumably resulting from the rupture of some fibers.

Before and during each ramp-shaped release, five x-ray diffraction images were recorded in defined time frames, with exposure times ranging from 2–4 ms (Fig. 2 *A*, *bottom*):

Time frame I: Image recorded under isometric steady-state conditions; exposure time, 3 ms; end of recording, 0.5 ms before the start of release.

Time frame II: Image recorded during the first rapid force decline but before the retardation of the force decline; start of exposure, 1 ms after the start of the ramp; exposure time, 2 ms (short exposure time to avoid cutting into the retardation of force decline).

Time frame III: Image recorded after the retardation of force decline, i.e., early in the second phase of force decline; start of exposure, 7.5 ms after the start of the ramp; exposure time, 3 ms. During this phase of release, maximum accumulation of cross-bridges in later states of the power stroke is expected (20).

Time frame IV: Image also recorded during the second phase of force decline immediately after time frame III (with a pause of $<$0.1 ms); start of exposure, ~10.5 ms after the start of the ramp; exposure time, 3 ms.

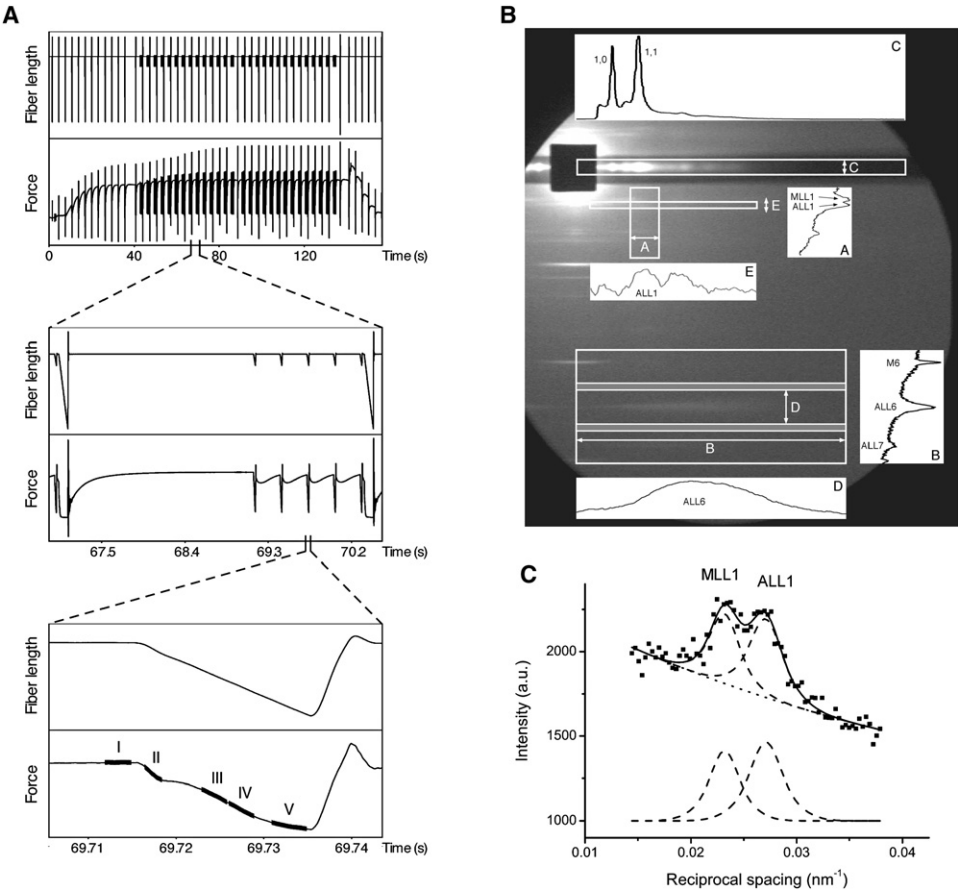

FIGURE 2 Experimental protocol and data analysis (a.u., arbitrary units). (*A*) Timing of mechanical maneuvers and collection of diffraction patterns. Example of one single-fiber array is given. (*A–C*, *top traces*) Fiber length. (*A–C*, *bottom traces*) Force. (*Top*) complete protocol (160 s) applied to each single-fiber array. Change to activating solution is indicated by small artifact on force trace ~5 s into the record. Change back to relaxing solution occurred at ~140 s. (*Middle*) Expanded view of one cycle of unloaded shortening, restretch with subsequent redevelopment of isometric force, and five ramp-shaped releases imposed after force had reached steady-state level. (*Bottom*) Expanded view of one ramp-shaped release followed by restretch to starting length. Bold sections of tension trace represent open times of x-ray shutter. I–V denote numbering of five time frames in which 2D x-ray diffraction patterns were recorded. (*B*) 2D x-ray diffraction pattern illustrating areas of interest (*A–E*) defined for generation of 1D intensity profiles. Within areas of interest, integration was performed by adding up intensities of pixels along column lines (*vertical direction*) or row lines (*horizontal direction*), as indicated by double arrows. Intensity profile across MLL1 and ALL1 (*area A*), and profile across ALL6 (*area B*), were obtained by horizontal integration along row lines. Profiles along equator (*area C*), along ALL6 (*area D*), and along ALL1 (*area E*) were obtained by vertical integration. For subtraction of background from profile along ALL6, intensities in two gray strips located alongside ALL6 were used. For further details, see text. (*C*, *top trace*) One-dimensional intensity profile of ALL1 with overlapping MLL1 of pattern recorded during frame III. Data points of profile (*solid squares*) were obtained by horizontal integration of area A, as defined in *B*. Continuous line describes fit of ALL1 and MLL1 with function that consists of sum of two bell-shaped curves, each consisting of two Gaussian functions, and one exponential decay for underlying background. Dashed lines indicate MLL1 and ALL1 profiles from fitting. Dotted line indicates background function. (*C*, *bottom traces*) MLL1 and ALL1 profiles from fitting after background subtraction.

Time frame V: Image recorded shortly before the end of ramp-shaped release; start of exposure, 15.5 ms after the start of the ramp; exposure time, 4 ms.

During each of the five consecutive release/restretch maneuvers, the data of time frames I–V had to be stored as separate frames (total of 5 × frames I–V = 25 frames). Data recorded in the 28 (or 20) consecutive cycles, separated by periods of unloaded shortening, were directly accumulated in the corresponding frames. To allow storage of the required total of 25 frames without exceeding the available memory, the data of each frame were binned 4:1 in a horizontal direction. As a result, upon unbinning, the intensity of one pixel was equally distributed among 4 adjacent pixels in a horizontal direction. Thus, in Fig. 1 *A*, each signal of an individual photon results in a 4-pixel-wide horizontal line. Even with this binning, however, the maximum number of frames that we could assign during ramp-shaped release/restretch maneuvers was limited, so that we had to select the most significant time periods for data recording, instead of defining a continuous series of adjacent time frames.

The whole experimental procedure was repeated with six single-fiber arrays during isometric contraction (pCa 4.5). For comparison, diffraction patterns with the same time frames and same timing protocol were recorded under relaxing conditions (four fiber arrays) and without nucleotides (rigor-conditions; five fiber arrays). Under relaxing conditions and in rigor, however, ramp-shaped length releases were not imposed, nor were fiber arrays unloaded, as was done with activated fibers.

Data reduction and analysis of time-resolved data

For each fiber array, the diffraction patterns recorded in corresponding time frames (I–V) of the five consecutive ramp-shaped releases were added up, yielding the summed-up frames I–V. The resulting five patterns of each fiber array were then corrected for the dead time of the detector using the DTC (dead time correction) routine, developed by the SRS (41). Next, the uneven sensitivity of the detector was compensated by dividing each image through a ''flat-field'' image recorded with the detector, while the beam was homogeneously scattered by air upon removal of the evacuated beam pipe between the specimen and the detector. Each pattern was then carefully rotated and centered, using the 1,0 equatorial and M3 meridional reflections as reference points. Finally, after these procedures, corresponding diffraction patterns of different fiber arrays were added up. To obtain comparable intensity levels for all time frames recorded under different conditions, the counts in each pixel were divided by 1), the number of arrays used for each condition (6 for active contraction, 4 for relaxing conditions, and 5 in rigor); and 2), by the duration of different time frames (2–4 ms) during which the patterns were recorded. For these procedures, programs of the CCP13 (Collaborative Computational project 13) software suite (http://www.fiber-diffraction.ac.uk/small-angle/Software.html) were used. Because the patterns had to be subjected to these normalization routines, the resulting ''counts'' in a pixel were no longer identical with the number of photons counted in the original patterns.

The signal/noise ratio for the first myosin and first actin layer line was further increased by folding the diffraction pattern across the equatorial axis. This was possible because the first actin and first myosin layer lines (ALL1 and MLL1, respectively) were still fully covered in the quadrant above the equator, whereas the rest of this quadrant fell outside the detected part of the pattern (Fig. 2 *B*). The scale for reciprocal spacing in diffraction patterns was calibrated by assuming that the position of the M3 reflection on the meridian for fibers in rigor condition is 1/14.43 nm^{-1} (10,42).

Generation of one-dimensional profiles

To generate one-dimensional (1D) intensity profiles, rectangular sections were defined, and intensities of pixels were integrated horizontally (parallel to the equator) or vertically (parallel to the meridian), using the BSL program of the CCP13 suite. To generate intensity profiles across part of ALL1 and MLL1, the rectangle, labeled *A* in Fig. 2 *B*, was defined and integrated horizontally. A resulting sample profile, labeled *A*, is included in Fig. 2 *B*. The integration covered the region from reciprocal spacing of 0.039–0.06 nm^{-1} (Fig. 2 *B*, *double arrow A*). This range was chosen because the increase in intensity of ALL1 upon isometric contraction is largest in this section (43). Moreover, in this range, actin and myosin components are well-separated from the first troponin reflection on a meridian at 1/38 nm^{-1}. Overall intensity profiles across ALL6 were generated by a horizontal integration of intensities within the large rectangular area labeled *B* in Fig. 2 *B*. A sample profile, labeled *B*, is also shown in Fig. 2 *B*. A 1D intensity profile along the equator covering the 1,0 and 1,1 reflections (Fig. 2 *B*, *sample profile C*) was obtained by vertical integration of the area labeled *C*.

To generate intensity profiles along ALL1 (Fig. 2 *B*, *sample profile E*), the intensity values of the 2D pattern were integrated vertically within area E from reciprocal axial spacing 0.025–0.029 nm^{-1}. The lower limit (0.025 nm^{-1}) was chosen to be half way between the axial positions of the first myosin and first actin layer line. From the resulting profiles the background was subtracted. The background function was determined by a double-exponential fit of 20 data points evenly distributed on both sides of the intensity peaks on the profile. The 20 data points were placed in parts of the profile that did not contain contributions from other reflections. After subtraction of the background from the 1D profiles of ALL1, the background-subtracted profiles of ALL1 were smoothed by a 15-point rolling average to reduce scatter.

Intensity profiles along ALL6 with background subtraction (Fig. 2 *B*, *sample profile D*) were obtained in the following way. Two strips, midway between the fifth and sixth actin layer lines and between the sixth and seventh actin layer lines, were defined as background. Their width was 0.0048 nm^{-1} for patterns recorded at the ESRF. These two background strips were integrated vertically, yielding 1D background profiles along ALL6. The two background profiles were added and smoothed by calculating a rolling average over 200 adjacent data points. To reduce noise further, the resulting background profiles of all five frames I–V were averaged. The area flanked by the two background strips, which is 0.02 nm^{-1} wide and contains ALL6 (Fig. 2 *B*, *area D*), was also integrated vertically to obtain a 1D profile. From the resulting 1D profile, the averaged background profile was subtracted. To reduce the noise of background-subtracted ALL6 profiles, profiles obtained after background subtraction were smoothed by a rolling average of 100 points. Such background subtraction for ALL6 was possible because in diffraction patterns recorded from rabbit psoas muscle fibers at low temperature (here, 5°C), myosin layer lines beyond MLL5 are essentially undetectable (32,42). Therefore, MLL7, which is very close to ALL6 (44), does not contribute significant intensity to the background defined here for ALL6.

Integrated intensities of equatorial 1,0 and 1,1 reflections, as well as of MLL1, ALL1, and ALL6, were determined by fitting a function consisting of the sum of an appropriate number of peak functions (one for each reflection or integrated layer line) and one exponential decay (for the background) to the 1D-intensity profiles, using the software package ORIGIN (OriginLab, Northampton, MA). An example for the fitting of MLL1 and ALL1 (Fig. 2 *B*, *profile A*) is given in Fig. 2 *C*. The area of each individual peak was obtained from the least-squares fit. Because the precise intensity profile of the x-ray beam is unknown, a peak function optimally fitting the data had to be constructed. The data were best fitted by a peak function consisting of the sum of two Gaussian functions at the same position, with the ratio of their area at 1.72:1 and the ratio of their width at 1.94:1. Application of single Gaussian or Lorentzian functions yielded higher χ^2 values (data not shown). For the fitting of equatorial reflections and of the sixth actin layer line, single Gaussian functions represented the data sufficiently well.

These procedures of data analysis were performed for patterns recorded in time frames I–V of the activated fiber arrays, and for patterns recorded under relaxing conditions and in rigor with the same time-frame protocol, except that no mechanical maneuvers were imposed. Individual patterns recorded in time frames I and V under relaxing conditions and in rigor were analyzed as described for patterns recorded from activated fiber arrays. The intensity values obtained from the five individual patterns were used to calculate mean values and standard deviations (population SDs, and not SDs of mean values) for both relaxed and rigor conditions. To obtain an estimate for the

error of intensities in time frames I–V of activated fibers, we used the SD values obtained for the corresponding intensities of patterns recorded in different time frames under relaxing and rigor conditions. Because the mean intensities were different for activated fibers versus relaxed and rigor fibers, we estimated the SD values for activated fibers by interpolation between the SDs of the relaxed and rigor data according to mean intensities (for all intensities analyzed in this work, the mean intensity of activated fibers was between relaxed and rigor intensities). We used this approach to estimate errors in the observed intensities of activated fibers where only one set of patterns was available. We did not use counting statistics, i.e., the square root of integrated intensities, as an error estimate, because we observed previously and in this study that the square root of integrated intensities is much smaller than the SD obtained when several diffraction patterns are recorded under identical conditions and analyzed individually. This finding is most likely attributable to the fact that errors, such as movements of fibers because of the pumping of solution, collections of patterns from slightly different parts of fiber arrays due to vertical scanning of a specimen in an x-ray beam, or uncertainties in dead-time and flat-field corrections, also contribute to the total error.

X-ray diffraction experiments with MgATPγS at SRS and HASYLAB

Two-dimensional x-ray diffraction patterns of single-fiber arrays were recorded without imposing length changes, under relaxing conditions, in rigor, and in the presence of 1000, 100, and 20 μM MgATPγS at a high Ca^{2+} concentration (pCa 4.5). For the ATPγS-experiments, Ap_5A (0.2 mM), hexokinase (0.5 U/mL), and glucose (200 mM) were added to remove traces of MgATP in the incubation medium. These data were recorded at beam line 2.1 of the SRS, using a position-sensitive multiwire detector, as described previously (16). Development of the single-fiber array method (32) and the recording of a similar data set under relaxing and rigor conditions, as well as in the presence of 1000, 100, and 20 μM MgATPγS, were performed at HASYLAB (Deutsches Elektronensynchrotron, Hamburg, Germany), using imaging plates and a BAS2000 Scanner (both Fujifilm, Tokyo, Japan).

Data reduction and analysis of MgATPγS-data

Diffraction patterns recorded at the SRS were corrected for unevenness of detector response, using a pattern obtained by irradiation of the detector with a ^{55}Fe radioactive source. All patterns recorded at the SRS were normalized to the intensity of the main beam, monitored through a semitransparent beam stop. Camera background, including solution scattering, was recorded after removal of the fiber array while the solution chamber was kept at its position in the x-ray beam. This camera background was subtracted from the recorded diffraction patterns. Subsequently, the background-subtracted patterns were rotated and centered as described for patterns recorded at the ESRF. Finally, the patterns were folded across the axes of equator and meridian, i.e., the intensities at corresponding positions in all four quadrants of a diffraction pattern were added up. To obtain final diffraction patterns for 1000, 100, and 20 μM MgATPγS, and two control patterns under the relaxing and rigor conditions shown here, patterns that had been recorded under all five conditions from five single-fiber arrays were added, after the above correction and centering procedures, to increase the signal/noise ratio.

One-dimensional profiles along the equator and ALL1, across MLL1 and ALL1, and across ALL6 were calculated by integrating corresponding areas at the same reciprocal spacings as used for time-resolved patterns recorded at the ESRF (Fig. 2 *B*). The intensities of the investigated reflections and layer lines were obtained by least-squares fitting, as described above. An error estimate for each fitted profile was obtained by the standard error of the fit, calculated by the fit program of ORIGIN (OriginLab). Because these diffraction patterns were recorded on imaging plates, no straightforward estimate of the number of actually collected photons was available. Thus, counting statistics could not be used for an error estimate. However, we do not attempt any quantitative inferences from a comparison of time-resolved data with the ATPγS-data.

Intensity profiles along ALL6 were obtained as described for the time-resolved data recorded at the ESRF, except that: 1), 0.0027 nm^{-1} was chosen as the width for the two strips along ALL6; 2), after the addition of the data of the two background profiles, the resulting profiles were smoothened by calculating a rolling average over 40 adjacent data points; 3), the width of the integrated strip between the two background strips that contained ALL6 was 0.028 nm^{-1}; and 4), the background-subtracted ALL6 profiles were smoothed by a rolling average of 20 data points.

RESULTS

Two-dimensional x-ray diffraction patterns

To identify features in the 2D x-ray diffraction patterns that are characteristic of an accumulation of cross-bridges in rigor or rigor-like conformations, we first recorded 2D patterns at decreasing concentrations of MgATPγS, an MgATP analog that is hydrolyzed only very slowly (33,45,46). When the MgATPγS concentration in the absence of MgATP is reduced, the fraction of nucleotide-free myosin heads in the rigor conformation increases, whereas the number of myosin heads with bound MgATPγS (i.e., in a weak-binding conformation) decreases (32,33). Fig. 3 shows one quadrant of 2D-patterns recorded with 1000, 100, and 20 μM MgATPγS, as well as in rigor (0 μM MgATPγS) and relaxing conditions. The most obvious changes, aside from changes on the equator, are: 1), the increasing enhancement of ALL1 with the characteristic lattice sampling (Fig. 3 *E*, *arrows*); and 2), enhancement of ALL6 near the meridian (Fig. 3). To identify features that are specific for the accumulation of rigor or rigor-like cross-bridges and thus are different or not seen when cross-bridges accumulate in force-generating states present during isometric contraction, we compared the changes evident at different MgATPγS concentrations with the changes seen in 2D patterns recorded under relaxing conditions and under isometric contraction at saturating Ca^{2+} concentrations (pCa 4.5). The relevant 2D patterns are shown in Fig. 4 *A* (isometric steady state) and Fig. 4 *D* (relaxing conditions). Compared with the rigor pattern (Fig. 4 *E*), the intensity of ALL1 in the isometric pattern is much lower, and ALL6 is also less intense. Fig. 4, *B* and *C*, shows two patterns recorded during ramp-shaped releases immediately after the start of the release (Fig. 4 *B*, time frame II), and after the presumed redistribution of cross-bridges at the end of the pause in force decline (Fig. 4 *C*, time frame III). For a detailed characterization of features specific to the accumulation of rigor or rigor-like cross-bridges and for a comparison with changes seen during ramp-shaped releases imposed during active contraction, we focused further analysis on equatorial reflections as well as ALL1 and ALL6.

Equatorial reflections

Individual intensities of the equatorial 1,0 and 1,1 reflections ($I_{1,0}$ and $I_{1,1}$, respectively) are shown in Fig. 5, *A–D*. $I_{1,0}$ is high under relaxing conditions, and low in rigor (Fig. 5,

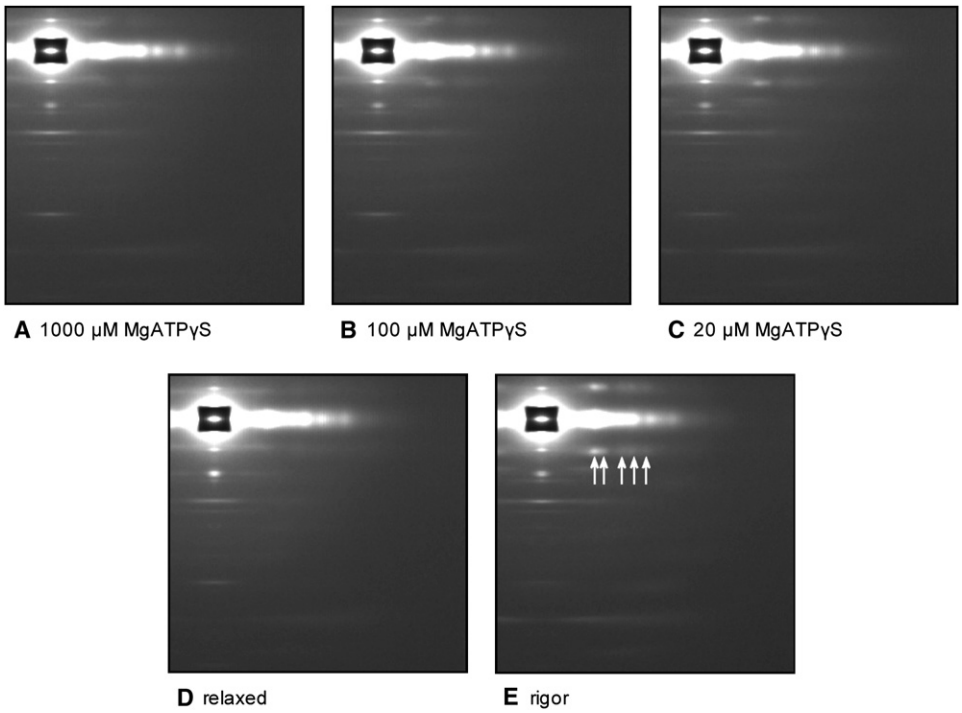

FIGURE 3 Static 2D x-ray diffraction patterns (no imposed length changes; SRS, Daresbury, Warrington, UK). (*A–C*) Different concentrations of MgATPγS at saturating [Ca^{2+}] (pCa 4.5). (*D*) Relaxing condition. (*E*) Without nucleotide (rigor). (*E*) Arrows indicate lattice sampling on ALL1.

A and *B*). From time frames I to V, recorded at maximum Ca^{2+} activation before and during ramp-shaped releases, a slight increase in $I_{1,0}$ is evident (Fig. 5 *A*), whereas with reduction in MgATPγS concentration, i.e., with an increasing fraction of nucleotide-free (rigor) cross-bridges, $I_{1,0}$ decreases (Fig. 5 *B*). $I_{1,1}$ is low under relaxing conditions, and high in rigor (Fig. 5, *C* and *D*). $I_{1,1}$ also rises somewhat from time frames I to V (Fig. 5 *C*), and shows a large increase when the MgATPγS concentration is reduced (Fig. 5 *D*).

The intensity ratio of the equatorial 1,0 and 1,1 reflections ($I_{1,1}/I_{1,0}$) was 2.9 in rigor, and 1.1 in relaxation, at the ESRF (Fig. 5 *E*), and 2.3 and 1.2, respectively, at the SRS (Fig. 5 *F*). $I_{1,1}/I_{1,0}$ increased steeply as MgATPγS was reduced (Fig. 5 *F*). In the time-resolved patterns of activated

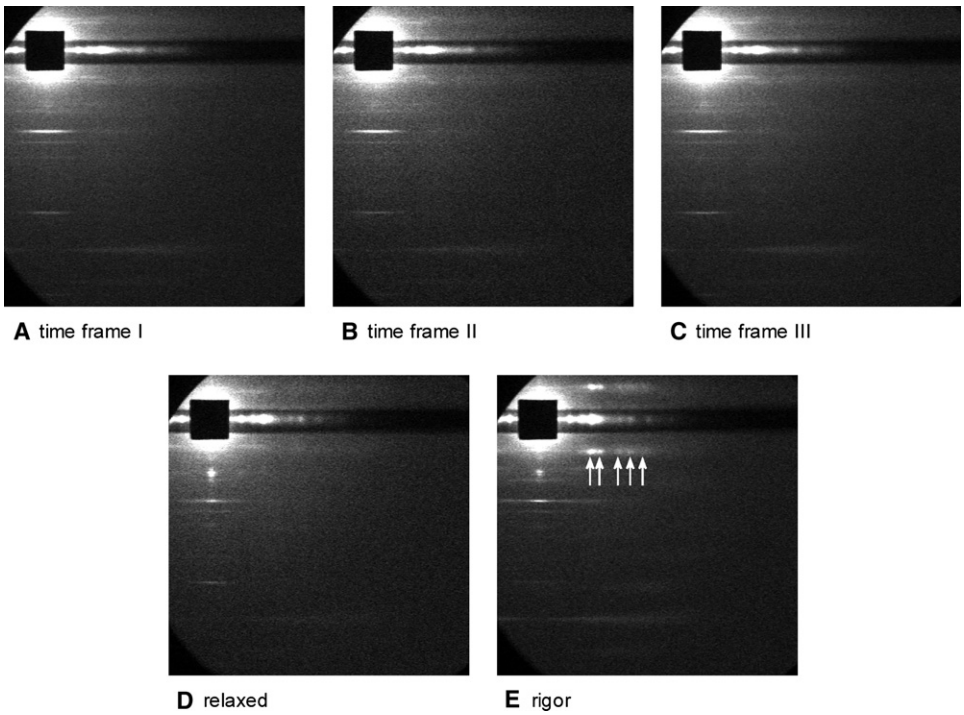

FIGURE 4 (*A–C*) 2D x-ray diffraction patterns recorded during isometric steady-state contraction and during ramp-shaped releases. Time-resolved experiments (ESRF, Grenoble, France). (*A*) Pattern taken before start of ramp-shaped release (isometric; time frame I). (*B*) Before pause in tension decline (time frame II). (*C*) After pause in tension decline (time frame III). (*D* and *E*) Patterns of fiber arrays under relaxing conditions and in rigor, respectively. (*E*) Arrows indicate lattice sampling on ALL1. Because of narrower focus of x-ray beam at ESRF ID02, reflections and lattice sampling in *E* are more distinct than in rigor pattern recorded at the SRS (Fig. 3 *E*).

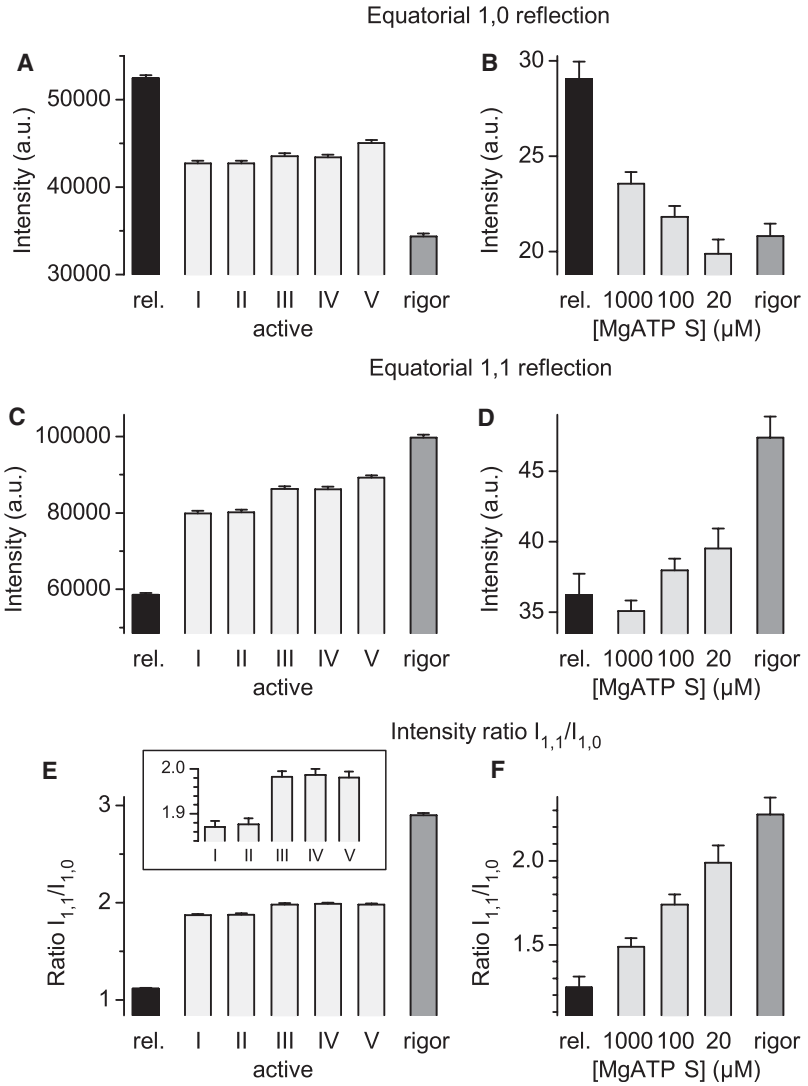

FIGURE 5 Intensities of equatorial 1,0 and 1,1 reflections ($I_{1,0}$ and $I_{1,1}$, respectively) and ratio of these intensities ($I_{1,1}/I_{1,0}$). (*A*, *C*, and *E*) Intensity values obtained in time-resolved recordings (ESRF, Grenoble, France) during active contraction in time frames I–V (*open bars*), under relaxing (rel.) conditions (*solid bars*), and in rigor (*gray bars*). (*E*, *inset*) $I_{1,1}/I_{1,0}$ for activated fibers in time frames I–V on expanded scale. Intensity values are in arbitrary units. (*B*, *D*, and *F*) Data of patterns recorded without imposing length changes (SRS, Daresbury, Warrington, UK) under relaxing conditions (1 mM MgATP; *solid bars*), with MgATPγS at pCa 4.5 (1000 μM, 100 μM, and 20 μM MgATPγS; *light gray bars*), and in rigor (*dark gray bars*). For details of error bars, see Materials and Methods. Error bars are sometimes smaller than symbol size.

fibers (Fig. 5 *E*), the $I_{1,1}/I_{1,0}$ values for the isometric condition (time frame I) and at the beginning of ramp-shaped release (time frame II) did not differ significantly. However, this was followed by a substantial increase in the $I_{1,1}/I_{1,0}$ ratio at the transition from time frame II to time frame III, from 1.87 to 1.98. The overall changes, however, were small compared with the change between patterns in rigor and under relaxing conditions, also recorded at the ESRF for reference. The changes in $I_{1,1}/I_{1,0}$ ratio at the transition from time frame II to time frame III are more clearly visible on the expanded scale of the inset in Fig. 5 *E*.

Because we had added all corresponding frames to maximize the signal intensity, we could not directly determine experimental error. The error bars for $I_{1,0}$, $I_{1,1}$, and $I_{1,1}/I_{1,0}$ in the time-resolved experiments with activated fibers were therefore derived from the scatter of intensity values of patterns recorded in different time frames when we applied the same time frame-recording protocol to fiber arrays in rigor and under relaxing conditions, but without imposing ramp-shaped releases (see Materials and Methods). Because the 1,0 and 1,1 reflections produced a very high signal on the detector, the error associated with the measured intensities was very low. For the ratio $I_{1,1}/I_{1,0}$, this error was ~0.7%. This is much lower than the change of nearly 6% in the $I_{1,1}/I_{1,0}$ ratio observed between time frame II and time frame III.

ALL1

In the MgATPγS-experiments, the intensity profiles along ALL1 (Fig. 6 *A*) showed a continuous increase in intensity as the concentration of MgATPγS was reduced from 1000 μM through 100 μM and 20 μM to 0 μM (rigor conditions). The intensity profile along ALL1 remained very similar as the concentration of MgATPγS was reduced (Fig. 6 *A*). It only appeared to be more and more scaled up.

The overall intensity of ALL1 in patterns recorded during isometric steady-state contraction, as well as during ramp-shaped releases, was much lower than in rigor (Fig. 4). To reveal possible differences in the intensity profile along ALL1 of activated fibers, Fig. 6 *B* shows such intensity profiles generated by a vertical integration of area E in

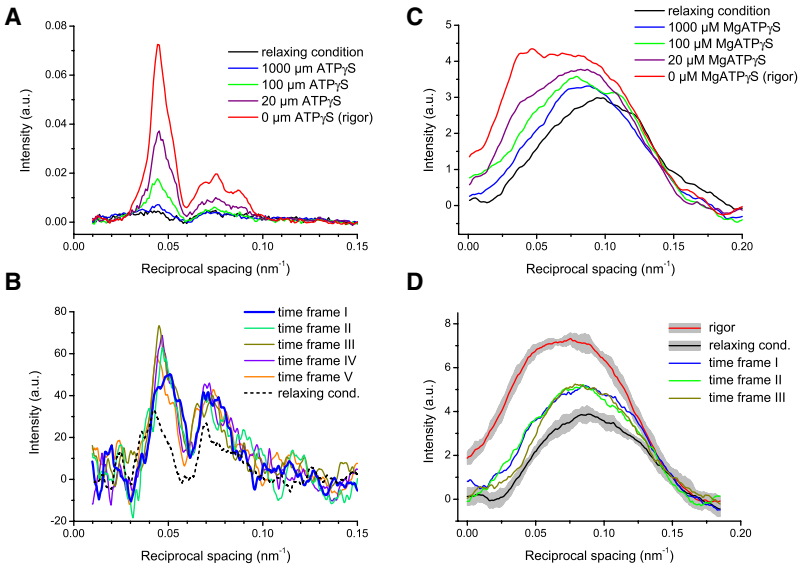

FIGURE 6 Intensity profiles along ALL1 and ALL6. Profiles were obtained by vertical integration of area E in Fig. 2 *B* for ALL1, and area D in Fig. 2 *B* for ALL6. All profiles are shown after background subtraction. (*A*) Profiles along ALL1 at different concentrations of MgATPγS, as well as under relaxing conditions and in rigor. (*B*) Intensity profiles along ALL1 recorded during isometric steady-state contraction (*time frame I*) and during ramp-shaped releases (*time frames II–V*). In addition, the profile for relaxing conditions is also shown (*dashed line*). The first peak on ALL1 of activated fibers changes shape at beginning of release, and stays essentially unchanged thereafter. Profile and intensity of second peak between 0.06–0.09 nm^{-1} reciprocal spacing remain essentially the same in frames I–V (within the scatter of the data). Relative intensities of first and second peaks of ALL1 in active contraction are near 1:1, whereas for the rigor profile (*A*), the intensity of the second peak is only ~50% of the first peak. (*C*) Intensity profiles along ALL6 at different MgATPγS concentrations, in rigor, and under relaxing conditions. Note sensitivity of ALL6 intensity profiles between inverse spacings of 0.02 and 0.10 nm^{-1} to concentration of MgATPγS, i.e., to fraction of cross-bridges in a nucleotide-free, rigor conformation. (*D*) Intensity profiles along ALL6 recorded in time frames I, II, and III. For comparison, profiles of rigor and relaxing conditions are shown. These two profiles represent mean values of individual profiles recorded in different time frames in rigor and relaxation, respectively (no releases imposed). Gray bands indicate standard deviation. Note distinct profile for time frame III versus time frames I and II between reciprocal spacings 0.025 and 0.06 nm^{-1}. Intensity profile of time frame IV (omitted for clarity) was essentially identical to profile of time frame III. Note intensification with shift toward meridian in time frames I and II when compared with relaxed profile, whereas profile in time frame III (and IV; not shown) shows intensification without shift toward meridian.

Fig. 2 *B*. The profile for relaxing conditions is also shown for comparison (Fig. 2 *B*, *dashed line*). All profiles show two broad peaks like those seen for the different MgATPγS concentrations. Under isometric conditions (frame I), the first peak, however, is rather flat and broad, but becomes narrower with the start of releases, i.e., in frames II–V. This shape change, however, does not significantly affect the total integrated intensity of the first peak of ALL1 (Fig. 7 *A*, *inset*).

The intensity profile of the second peak on ALL1 between 0.06 and ~0.09 nm^{-1} reciprocal spacing is essentially unchanged within the scatter of the data in frames I–V (Fig. 6 *B*). Quite importantly, however, the intensity ratio between the first and second peak in profiles from activated fibers (frames I–V) is very different from the ratio in the rigor profile. In rigor, the intensity of the second peak relative to the first peak is much lower. Altogether, the intensity distribution along ALL1 changes during ramp-shaped releases, but does not change toward the rigor-type profile (intensities of first versus second peak).

For quantification, Fig. 7, *A* and *B*, shows the integrated intensity of the most intense part of ALL1 (first peak of the intensity profile along ALL1; cf. Fig. 2 *B*, *area A*) in the different time frames of activated fibers (Fig. 7 *A*), and at different MgATPγS concentrations (Fig. 7 *B*). The ALL1 intensities in rigor and relaxation are also shown for reference. The integrated intensity of the most intense part of ALL1 of activated fibers (Fig. 7 *A*) is ~2.5-fold higher than under relaxing conditions, as shown elsewhere (16). Under rigor conditions, the intensity of ALL1 is ~20-fold larger than during relaxation. Accordingly, an increasing intensity of the first peak of the intensity profile of ALL1 is found when the MgATPγS concentration is reduced (Fig. 7 *B*). This very large increase in ALL1 intensity in rigor and when the MgATPγS concentration is reduced reflects the increasing number of stereospecifically attached nucleotide-free myosin heads (47,48). Compared with the large intensity increase of ALL1 in rigor and at low MgATPγS concentrations, only rather small intensity changes of ALL1 are seen through time frames II–V of ramp-shaped releases of activated fibers. Thus, a significant change in the number of stereospecifically attached myosin heads, and particularly of heads in a rigor-like conformation, cannot be inferred from the observed intensities in time frames I–V.

ALL6

The total integrated intensity of the sixth actin layer line (Fig. 7, *C* and *D*) was obtained from intensity profiles of area B (Fig. 2 *B*, *sample profile B*), as described in Materials and Methods. During active contraction, ALL6 intensity is ~40% higher than under relaxing conditions, as shown previously (10,16). In rigor, the integrated intensity is about double the intensity seen under relaxing conditions, at least for the direct comparison at the ESRF. The total ALL6 intensity for activated fibers shows a slight decrease in the course from time frame I to time frame V. With decreasing MgATPγS concentration and hence an increasing proportion of myosin heads attached to actin in rigor-like conformation, an increase in integrated ALL6 intensity is evident (Fig. 7 *D*).

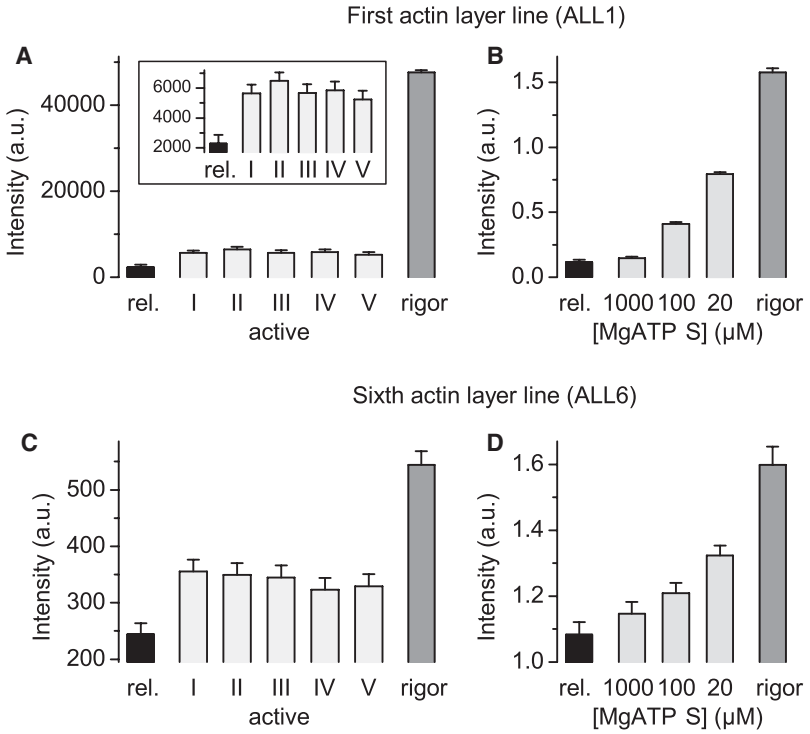

FIGURE 7 Integrated intensities of ALL1 and ALL6. Intensities obtained by horizontal integration of layer lines within rectangular areas labeled *A* and *B* in Fig. 2 *B* for ALL1 and ALL6, respectively (a.u., arbitrary units). (*A* and *C*) Open bars, intensity values obtained from Ca^{2+}-activated fibers in time frames I–V; gray bars, intensity in rigor; black bars, intensities under relaxing conditions. (*A*, *inset*) Intensities of ALL1 for relaxed and activated fibers on expanded scale. (*B* and *D*) Intensity values from patterns recorded at different MgATPγS concentrations (*light gray bars*), in rigor (*dark gray bars*), and during relaxation (*rel.*) (*black bars*). For details of error bars, see Materials and Methods. Data are scaled such that intensity changes evident during ramp-shaped releases can be compared directly to intensity changes because of an increasing fraction of nucleotide-free, rigor cross-bridges when lowering MgATPγS concentration. Sarcomere length for MgATPγS titration was set at 2.5–2.6 μm to prevent quivering of fibers with pumping of solution at 1000 μM MgATPγS. Thus, changes from relaxation to rigor are somewhat smaller than in data from the ESRF (Grenoble, France).

The actually observed slight decrease of total ALL6 intensity from time frames I to V during releases of activated fibers is therefore the opposite of the change expected for an accumulation of cross-bridges in a rigor-like conformation.

Analysis of the intensity profile along ALL6, i.e., in the direction parallel to the equator (Fig. 2 *B*, *area D*, and *sample profile D*), revealed that with more rigor-like cross-bridges upon reduction of MgATPγS, an enhancement of ALL6 occurs near the meridian at inverse spacings from 0.03 nm^{-1} to 0.07 nm^{-1} (Fig. 6 *C* in Kraft et al. (16)). For the part of the intensity profile at reciprocal spacings >0.10 nm^{-1}, intensity is mostly unaffected by the proportion of rigor versus weakly bound cross-bridges. Altogether, Fig. 6 *C* indicates a positive correlation between the proportion of cross-bridges with rigor-like conformation and ALL6 intensification near the meridian.

Fig. 6 *D* shows ALL6 profiles for isometric steady-state contraction (time frame I) and during ramp-shaped length releases (time frames II and III). The profiles for time frames IV and V are omitted for clarity. The intensity profiles along ALL6 show distinct differences, depending on the time frame in which they were recorded. Whereas the profiles for time frames I (isometric) and II (before delay in tension decay) are very similar, the profile of time frame III shows lower intensities for reciprocal spacings up to 0.07 nm^{-1}, as does time frame IV (not shown in Fig. 6 *D*; see Table 1). This decrease of intensity is contrary to the increased intensity that would have been expected if an increasing number of cross-bridges with rigor-like conformation (Fig. 6 *C*) contributed to the intensity profile in time frames III and IV. Compared with relaxing conditions, the ALL6 profile for isometric steady state (time frame I) and in the ramp-shaped release before the pause in the tension decline (time frame II) appears to be enhanced and shifted toward the meridian. In contrast, for time frames III and IV (i.e., after the pause in the tension decline), the intensity profile along ALL6 appears enhanced compared with relaxing conditions, but without a shift toward the meridian. The gray bands encompassing average profiles for rigor and relaxation in Fig. 6 *D* show the scatter on these data resulting from data recording and analysis. This scatter was derived from the variability of individual profiles in rigor and relaxation obtained from patterns recorded with the same time-frame protocol as used in active contraction, but without any length change (see Materials and Methods).

TABLE 1 ALL6 intensities of activated fibers in time frames I–V

Time frame No.	Integrated intensity in interval 0.03–0.07 nm^{-1} ± SD
I	53.45 ± 2.46
II	53.89 ± 2.46
III	47.13 ± 2.46
IV	46.12 ± 2.46
V	49.28 ± 2.46

Intensity values were obtained by integration of near-meridional part (0.03–0.07 nm^{-1} reciprocal spacing) of ALL6 profiles (see Fig. 6 *D*). Intensities are expressed in arbitrary units. Standard deviations (SDs) for time frames recorded in active contraction were obtained by interpolation between SDs of rigor and relaxed profiles, weighted by respective mean values of integrated intensities.

For a further analysis of the intensity changes of the near-meridional part of ALL6 for time frames I–V of activated fibers, integrated intensities between 0.03–0.07 nm^{-1} reciprocal radial spacings were obtained (Table 1). This interval was chosen because MgATPγS titration (Fig. 6 *C*) showed a positive correlation between the proportion of rigor-like cross-bridges and the intensity within this interval. The values in Table 1 indicate for activated fibers that the integrated intensity between 0.03–0.07 nm^{-1} drops substantially from time frame II to time frame III. As a consequence, the ALL6 profile in frame III (and frame IV) appears vertically scaled up from the relaxed profile, without a shift toward the meridian (Fig. 6 *D*). This change coincides with the end of retardation in the tension decline during ramp-shaped length release (Fig. 2 *A*, *bottom trace*), which is thought mainly to reflect a redistribution of cross-bridges toward later states of the power stroke.

DISCUSSION

Several concepts predict that cross-bridge states with rigor or rigor-like structural features are the main states in which cross-bridges contribute to the generation of isometric force (5–9). In contrast, 2D x-ray diffraction patterns (10–18), electron microscopy (49), and mechanical studies (22–25) are consistent with a concept derived from studies of force transients in response to ramp-shaped length changes (20,21), in which isometric force is generated by cross-bridges in early states of the power stroke that do not show rigor or rigor-like structural features. According to this concept, as supported by more recent studies that used x-ray diffraction combined with mechanical (15) or T-jump (17) perturbations, cross-bridges are expected to accumulate only in rigor or rigor-like states when driven to late states in their power stroke, e.g., by length releases imposed on isometrically contracting fibers. In this study, we tested whether the appearance of rigor or rigor-like structural features can be detected in 2D x-ray diffraction patterns recorded during ramp-shaped length releases.

Changes in 2D x-ray patterns specific for accumulation of rigor or rigor-like cross-bridges

To find out which changes in 2D x-ray diffraction patterns allow us to answer the question about possible accumulation of rigor or rigor-like cross-bridges in response to length releases imposed on actively contracting fibers, we first had to identify features that are specific to an increase in the number of rigor(-like) cross-bridges. We studied 2D x-ray patterns when, upon reduction of MgATPγS concentration, more and more cross-bridges change from weak-binding states to the nucleotide-free rigor state, and compared the observed changes with differences seen between relaxed patterns and patterns recorded during isometric steady-state contraction, i.e., when cross-bridges change from weak-binding states to strong-binding, force-generating states.

Intensity profile along ALL1

As shown in Fig. 6, the intensity profile along ALL1 seen in rigor is characterized by two broad intensity peaks. A first peak is located between inverse spacings 0.03 nm^{-1} and 0.06 nm^{-1}. Its integrated intensity is about twice the integrated intensity of the second peak between inverse spacings 0.06 nm^{-1} and 0.10 nm^{-1}. These two peaks and their 2:1 intensity ratio appear to be maintained when the number of cross-bridges in the nucleotide-free rigor state is reduced by increasing MgATPγS concentrations (Fig. 6 *A*). Only the magnitude of total ALL1 intensity appears to change. This feature of the intensity profile along ALL1 seen with rigor cross-bridges, however, is different from the profile recorded under isometric steady-state conditions (Fig. 6 *B*, time frame I; see also Kraft et al. (16)), where the second peak in the ALL1 intensity profile is essentially as large as the first, even if only the intensity increase from relaxing conditions (Fig. 6 *B*, *dashed line*) to isometric steady-state contraction (time frame I; Fig. 6 *B*, *blue solid line*) is considered. Thus, the ALL1 intensity profile appears to be one feature that distinguishes the formation of stereospecific rigor cross-bridges from stereospecifically attached cross-bridges during isometric contraction.

Intensity profile along ALL6

As the ATPγS concentration is reduced, the intensity of ALL6 increases, especially near the meridian (Fig. 6 *C*). For all MgATPγS concentrations, the maximum of the intensity increase on ALL6 was found around inverse spacings of 0.04–0.05 nm^{-1} (Fig. 4 *A* in Kraft et al. (16)). Under isometric steady-state conditions, intensity is increased from relaxed intensity over a broader range with a center of gravity around an inverse spacing of 0.07 nm^{-1} (Fig. 4 *B* in Kraft et al. (16)). Thus, based on ATPγS titration, the accumulation of cross-bridges in rigor or rigor-like states is expected to enhance the near-meridional intensity of the ALL6 profile.

Equatorial intensities

The intensity ratio $I_{1,1}/I_{1,0}$ of the equatorial 1,1 and 1,0 reflections increases both when rigor cross-bridges are formed and when fibers are activated under isometric conditions. Moreover, the absolute intensities $I_{1,1}$ and $I_{1,0}$ show a reciprocal change, both upon formation of rigor cross-bridges and when fibers are activated under isometric conditions, i.e., when the number of force-generating cross-bridges increases. The magnitude of changes in $I_{1,1}/I_{1,0}$, and of the reciprocal change in individual intensities, however, is lower when fibers are isometrically activated (50,51) (Fig. 5, *A* and *C*, versus Fig. 5, *B* and *D*). The

$I_{1,1}/I_{1,0}$ ratio, as well as individual intensities $I_{1,1}$ and $I_{1,0}$, however, were also found to be sensitive to changes in lattice order/disorder (50), e.g., when strain on the filament lattice changes. All three parameters were found to decrease with increasing lattice disorder (50). The effects on the intensity ratio and individual intensities, however, depend on the kind of disorder, i.e., the first or second kind (52). Thus, changes in equatorial intensity ratio and individual intensities do not allow unambiguous interpretation in terms of the accumulation of cross-bridges in rigor or rigor-like states versus accumulation in other strong-binding states that are occupied during isometric contraction.

Altogether, 1), the characteristic ~2-fold higher intensity of the inner versus outer peak on the intensity profile along ALL1, and 2), the intensification closer to the meridian of ALL6, are features by which rigor cross-bridges can be distinguished from strong-binding cross-bridges during isometric steady-state contraction.

Structural features of cross-bridges during ramp-shaped releases

In continuation of our previous work (20,21), we imposed ramp-shaped length releases on fibers in isometric steady-state contraction, and characterized structural features of cross-bridges that had accumulated at the time of the end of the delay in the tension decline seen during ramp-shaped releases (Fig. 2 *A*, *bottom*, frame III). We selected this approach because the slope of ramp-shaped releases can be adjusted such that the retardation of tension decay is most prominent and, at our experimental temperature of 5°C, well-separated from the start of ramp-shaped releases. This allowed us to place a time frame after the beginning of the release, but before the delay in tension decline (Fig. 2 *A*, *bottom*, frame II). Thus, during frame II, half-sarcomere strain, and thus cross-bridge strain, is already reduced, compared with isometric steady-state conditions, whereas the redistribution of cross-bridges among force-generating states is still very small (see below). We also selected this approach because the retardation in tension decline during ramp-shaped releases mostly signifies a redistribution of cross-bridges from the earliest state(s) of the power stroke to later states in the power stroke. Under our conditions (5 °C, amplitude of ramp-shaped release $\leq$20 nm/half-sarcomere, duration of 20 ms), the retardation of tension decline occurs between $\leq$2–8 nm/half-sarcomere of the length release (Fig. 2 *A*, *bottom*). This most likely is an upper limit, because it is determined from the change in overall fiber length. Thus, part of the length change will be taken up by the end compliances introduced by the attachment of the fibers to the motor and force transducer. In our experiments, the effects of end compliances appear to contribute no more than 10% to the observed overall length change. This estimate results from measurements with single skinned fibers in which the same ramp-shaped releases were applied, and the resulting change in sarcomere length was recorded by ''ω-averaged'' laser light diffraction (20,53). The ''ω-averaging'' was found to be essential for obtaining a representative sarcomere length signal with laser light diffraction, because of the domain organization of the contractile apparatus (54,55).

In our previous work with ramp-shaped length releases, a first distinct, nonsymmetric force response was evident when comparing ramp-shaped releases with ramp-shaped stretches, both imposed on isometrically contracting fibers. A retardation in the tension response was prominent only during releases, whereas for stretches from an isometric steady state, a similar retardation was much smaller or undetectable (cf. Fig. 1 *b* in Brenner (20)). A second distinct difference in force responses was observed when ramp-shaped stretches imposed during isometric steady-state contraction were compared with ramp-shaped restretches imposed in the course of a ramp-shaped release after the retardation in tension decline (cf. Fig. 2 *a* in Brenner (20)). During such restretches, a retardation as prominent in the tension response as during releases was evident. A model simulation of these observations implied that during isometric steady-state contraction, force is mainly generated in early states of the power stroke, whereas later states contribute much less. More precisely, the observed data were consistent with a 10:1 occupancy of states before versus after the step(s) postulated by Huxley and Simmons (19) to account for quick tension recovery in response to stepwise length changes (states A and B, respectively, in Brenner (20) and Brenner et al. (21)). Our modeling of the observed data furthermore implied that cross-bridges in state(s) before the transition responsible for quick tension recovery in response to stepwise length changes (or responsible for the delay in tension decline in ramp-shaped releases) generate $\geq$75% of isometric tension (20,21). Our previous model simulations further showed that the retardation in tension decay during ramp-shaped releases mostly results from a redistribution of force-generating cross-bridges from early states of the power stroke to later states in the power stroke, whereas new cross-bridges entering the force-generating states, or cross-bridges leaving later states in the power stroke, apparently become relevant only later in the ramp-shaped release, when the extent of filament-sliding exceeds 10–12 nm. These findings resulted from modeling the force responses to ramp-shaped length changes (cf. Figs. 1 *a* and 2 *b* in Brenner (20)), and are supported by recent x-ray diffraction and mechanical studies of isotonic transients (56). These studies implied that in response to load steps down to low steady-state forces (e.g., 14% of isometric force), cross-bridges will detach from their actin binding sites only after filament-sliding goes beyond 10–12 nm. Only then do strongly bound cross-bridges appear to leave the force-generating states, with new cross-bridges attaching to actin, i.e., entering force-generating states (56). As implied in Fig. 2 *A* (*bottom*), in large-amplitude ramp-shaped releases

with a slope of 1 nm/half-sarcomere per ms, as applied in this study, force would approach a steady-state level of ~10–15% of isometric force. This steady-state level, as characterized by a much lower fraction of cross-bridges in strong-binding states (56–58), has not yet been achieved in our ramp-shaped releases. This is indicated by the intensity of ALL1 that has not yet changed much toward the relaxed value in the ramp-shaped releases used here (Fig. 7 *A*), whereas in the isotonic steady state, ALL1 is much reduced compared with isometric contraction (43).

In other models proposed to account for force responses during ramp-shaped stretches and releases (59,60), the occupancy of ''poststroke'' heads during an isometric steady state was assumed to be as high as 40%, with 60% of the actin-attached heads in the ''prestroke'' conformation. The ''poststroke'' heads were assumed to contribute almost 80% of isometric force. With such occupancies and such contributions to isometric force, we could not account for the force responses in our previous work (20,21). It remains to be clarified in future work whether these differences are attributable to different experimental conditions, or result from focusing on different experimental features when optimizing the model responses.

Nevertheless, based on our previous mechanical work and its modeling, the changes in intensity distribution along ALL1 and ALL6 from time frame II to time frame III (and IV) seen in this work under the same experimental conditions, and with the same muscle fibers, most likely reflect structural changes associated with a redistribution of cross-bridges from early states in the power stroke toward later states in the power stroke. Only minor contributions are expected from cross-bridges newly entering or finally leaving the strong-binding states associated with the power stroke.

2D patterns indicate an almost constant number of strong-binding cross-bridges in early part of ramp-shaped releases

No statistically significant changes in total integrated intensity of ALL1 and ALL6 were found during ramp-shaped releases (Fig. 7, *A* and *C*, time frames I–V). According to modeling work (47,48), this implies that the number of strong-binding cross-bridges does not change significantly during the retardation of tension declines in ramp-shaped releases. However, later in ramp-shaped length releases of longer duration than were used here, the redistribution of cross-bridges toward an isotonic steady state with a lower number of strong-binding cross-bridges will occur (58).

2D patterns recorded during ramp-shaped length releases do not reveal appearance of features of rigor or rigor-like cross-bridges

In light of changes in 2D x-ray diffraction patterns specific to the formation of rigor (or rigor-like) cross-bridges, our most important findings in the 2D patterns recorded during ramp-shaped length releases are: 1), a lack of decrease in the outer peak of the intensity profile along ALL1, specifically in time frame III (Fig. 6 *B*); and 2), a lack of increase, but rather a decrease, in intensity near the meridian on ALL6 from time frame II to time frames III and IV (Fig. 6 *D*). Equatorial intensities, i.e., intensity ratio $I_{1,1}/I_{1,0}$ and individual intensities $I_{1,1}$ and $I_{1,0}$, do not allow for straightforward interpretation. If cross-bridges accumulated in rigor or rigor-like states, the expected increase in the I_{11}/I_{10} intensity ratio would be associated with a decrease in $I_{1,0}$, whereas $I_{1,1}$ would change only very little (14). Instead, we found an increase in both individual intensities (Fig. 5, *A* and *C*). This very likely resulted from an increase in lattice order when strain on the filament lattice was released as active tension decreased during ramp-shaped releases (50). Thus, a possible redistribution of strong-binding cross-bridges to structurally different states very likely was masked by lattice-disorder effects. From the intensity distribution along ALL1 and ALL6 during ramp-shaped releases, however, we conclude that there is no evidence for a redistribution of cross-bridges toward rigor or rigor-like states that is sufficiently large to result in detectable changes in 2D x-ray diffraction patterns characteristic of rigor(-like) cross-bridge conformations. A small redistribution below the detection limit, however, cannot be ruled out.

Evidence for the accumulation of cross-bridges in an as yet structurally unidentified state

Different from the expected intensity increase in ALL6 upon the accumulation of cross-bridges in rigor(-like) states, we found a decrease in the near-meridional part of the ALL6 intensity profile after the delay in tension decline of ramp-shaped releases. This not only argues against a redistribution toward rigor(-like) states, but suggests a redistribution of cross-bridges toward a so far structurally unidentified strong-binding state during ramp-shaped releases.

As shown by a comparison of experimental data (MgATPγS data versus isometric contractions; Fig. 6 *C* versus Fig. 6 *D*; also see Kraft et al. (16)), as well as by model calculations (47), the intensity profile along ALL6 is quite sensitive to structural changes of the actomyosin cross-bridge. This is specifically true for the near-meridional part of ALL6 from inverse spacing 0.03 nm^{-1} to 0.07 nm^{-1}. We therefore investigated whether the decrease in integrated intensity within this interval observed from time frames II to III (and time frame IV; see Table 1) is statistically significant or is purely attributable to the scatter of the data. To judge statistical significance, we compared the decrease in integrated intensity from time frame II to time frame III with the scatter in the integrated intensities. As a measure of scatter, we used the scatter observed among the data of individual frames when time-resolved 2D diffraction patterns were recorded from fiber arrays under relaxing and rigor conditions. For relaxing and rigor conditions, the

same timing of frames was applied as was used to record time-resolved patterns during active contractions. However, no ramp-shaped length changes were imposed. Consequently, the scatter in intensity among the different time frames of one condition (rigor or relaxation) reflects the degree of noise in data -recording and analysis procedures. We found standard deviations for the integrated intensities of the near-meridional segment of the ALL6 intensity profile of ± 2.11 and ± 2.61 under relaxing and rigor conditions, respectively. As an estimate for the standard deviation of time-resolved data recorded under activating conditions, we used ± 2.46. This was obtained by interpolation between the standard deviations ± 2.11 and ± 2.61, weighted by the associated mean values of the integrated intensities. With this estimate of the standard deviation, a one-sided Gaussian test was performed. This allowed us to examine whether the observed decrease was accidental or statistically significant. This test yielded a p-value of 0.026. With this p-value, the intensity decrease from time frame II to time frame III was statistically significant. That the observed decrease was not accidental is further supported by the fact that the profile in time frame IV is very similar to the profile in time frame III, with an integrated intensity of the near-meridional part that is even slightly lower (Table 1).

We conclude that the recorded intensity profiles along ALL6 argue against a substantial increase in the fraction of rigor(-like) cross-bridges. Our data imply instead that during the tension plateau seen in ramp-shaped releases, cross-bridges redistribute within the strong-binding states of the power stroke, accumulating in states that are characterized by a near-meridional intensity on ALL6 that is not only much lower than is seen in rigor, but is also lower than what is seen during isometric steady-state contractions.

What are the structural features of the presumed new intermediate?

The near-meridional part of ALL6 is affected by the light-chain binding domain. This was shown experimentally by Kraft et al. (16), using: 1), truncated S1, which included only the motor domain of the myosin head; and 2), *N*-ethyl-maleimide (NEM)-modified S1, which includes both the motor domain and the light-chain binding domain of the myosin head. The intensity maximum of ALL6 in diffraction patterns recorded from fibers with actin filaments decorated by NEM-S1 was nearer the meridian than when actin filaments were decorated with truncated S1. Actin filaments of skinned fibers decorated, in the absence of MgATP, with truncated S1 versus NEM-S1 mimicked states, for instance, with disoriented versus uniformly oriented neck regions, respectively. Therefore, the observed reduction in near-meridional intensity of ALL6 could originate from less well-ordered light-chain binding domains, i.e., from a larger ''spread'' of orientations, after cross-bridges were redistributed during the delay in tension decline of ramp-shaped releases. This possibility, however, is considered less likely, based on studies of interference fine structure of the first-order and second-order meridional reflection of myosin heads (M3 and M6) (18). In our study, we concluded that after quick tension recovery, i.e., after the equivalent of the retardation of tension decline in ramp-shaped releases, the distribution of cross-bridges remained essentially as narrow as under isometric conditions (18). Alternatively, the observed decrease in near-meridional intensity on ALL6 could indicate a different orientation of the light-chain binding domain after cross-bridge redistribution. The accumulation of cross-bridges in an ''antirigor-like'' conformation, e.g., when new cross-bridges enter the power stoke, is unlikely to cause the observed decrease in near-meridional intensity of ALL6. According to the model of Koubassova and Tsaturyan (47), such antirigor conformation produces a higher intensity of ALL6 near the meridian, as does the rigor conformation. A conformation somewhat less extreme than this ''antirigor'' conformation may be a suitable model for the conformation of cross-bridges during the generation of isometric force in early states of the power stroke. The redistribution of cross-bridges during the pause in tension decline toward a conformation with a more perpendicular orientation of the lever arm may, according to the model of Koubassova and Tsaturyan (47) and Koubassova et al. (48), generate a lower intensity on ALL6 between inverse spacings of 0.03–0.07 nm^{-1}.

It may be argued that nonzero average strain on rigor (-like) cross-bridges may generate the decrease in intensity of the near-meridional part of ALL6. This seems unlikely, because the ALL6 profiles of frames III and IV are essentially indistinguishable, with a nearly identical integrated intensity of the near-meridional part (Table 1), although active force during frame IV is only ~2/3 of the active force in frame III, and filament-sliding from frame III to IV is ~3 nm. Thus, the average cross-bridge strain in frame IV is clearly less than in frame III, whereas the near-meridional part of ALL6 is unchanged. A definitive answer regarding this point, however, must be left to future studies in which intensity profiles along ALL6 are compared in terms of rigor cross-bridges under different strains. We also cannot rule out that, instead of a different orientation of the light-chain binding domain, some change in actin conformation could cause the lower intensity on ALL6 between inverse spacings of 0.03–0.07 nm^{-1}. This would still be consistent with the general notion that the reduction in intensity of the near-meridional part of ALL6 is caused by a change in conformation of the actomyosin cross-bridge. Detailed conclusions must be left to future studies in regard to whether changes in orientation of the light-chain binding domain, or changes in the conformation of the actin monomer, or even changes in other parts of the myosin head domain, are the cause of the lower intensity of the near-meridional part of ALL6.

Implications of our findings

Our data strongly suggest that the conformational states accumulated during time frames III–V are neither rigor nor rigor-like. The lack of detectable accumulation of cross-bridges in the nucleotide-free rigor state, however, is not surprising, because this state is thought to be short-lived in the presence of physiological, i.e., millimolar, ATP concentrations. Our data also rule out accumulation in an ADP intermediate with rigor-like features. Such an AM.ADP-state with rigor-like structural features is seen when ADP is added to nucleotide-free rigor fibers (39). This state, however, may only represent the last intermediate just before ADP is finally released. Because no rigor-like structural features appear during ramp-shaped releases, this state apparently is also only short-lived, or may not occur at all on the normal ATPase pathway. Our data do not rule out the possibility that the state in which cross-bridges accumulate during the tension plateau in ramp-shaped releases, and which is characterized by the decreased near-meridional intensity on ALL6, is biochemically an AM.ADP intermediate, with structural features different from those of rigor cross-bridges, e.g., with an orientation of the light-chain binding domain more perpendicular to the fiber axis.

Relationship to previous work

Previous 2D x-ray diffraction work addressing effects on actin-based layer lines in response to stepwise or ramp-shaped length changes was reported by Yagi et al. (61). In their experiments, however, only integrated intensities of parts of ALL1 and of ALL6 were analyzed. The ranges of integration in their work closely correspond to our areas of integration. Our results for integrated intensities, in principle, agree with theirs. On ALL1, Yagi et al. (61) saw an increase in integrated intensity by ~10–15%, 2 ms after a stepwise length release. We saw an ~15% increase in integrated intensity in frame II, i.e., ~2 ms into the ramp-shaped release. In our data, this increase, however, was not statistically significant. For ALL6, Yagi et al. (61) reported a slow decease in integrated intensity by ~14%, whereas we saw only a trend toward a slow decrease of $<10\%$ that was also not statistically significant. Thus, our data are qualitatively consistent with those of Yagi et al. (61).

Our conclusion that, even upon length releases, cross-bridges do not accumulate in late, rigor(like) states of their working stroke is consistent with conclusions drawn from recordings of intensity and interference fringes of first-order and second-order meridional reflections of myosin heads (M3 and M6 (18)). Here we conclude that cross-bridges maintain a rather narrow distribution that is progressively moved through the working stroke as the length-release is increased, i.e., at different amplitudes of release, we may probe different conformations of force-generating cross-bridges as they are moved through their working stroke. Thus, the decrease that we observed in near-meridional intensity on ALL6 after the pause in the tension decline may be the first sight of a new state in the working stroke that is passed through, subsequent to the states occupied in isometric steady state. Whether this state is indeed characterized by a more perpendicular orientation of the light-chain binding domain, i.e., intermediate between a more antirigor-like orientation in early states of the power stroke occupied during isometric contraction and rigor-like states at the end of the cross-bridge working stroke, requires additional experimentation and more detailed modeling.

We thank T. Narayanan, P. Panine, (ESRF, Grenoble, France), S. Slawson (SRS Daresbury, Warrington, UK), and S. Funari (HASYLAB, DESY, Hamburg, Germany) for invaluable technical help at their respective beam lines. B. Piep, T. Beier, and A. Lingk (Department of Molecular and Cell Physiology, Hannover Medical School, Hannover, Germany) are acknowledged for excellent technical support.

The work was supported by the ESRF, SRS, DESY, and Deutsche Forschungsgemeinschaft (Kr 1187/18-1,2).

REFERENCES

1. Lymn, R. W., and E. W. Taylor. 1971. Mechanism of adenosine triphosphate hydrolysis by actomyosin. *Biochemistry.* 10:4617–4624.
2. Reedy, M. K., K. C. Holmes, and R. T. Tregear. 1965. Induced changes in orientation of the cross-bridges of glycerinated insect flight muscle. *Nature.* 207:1276–1280.
3. Huxley, H. E. 1969. The mechanism of muscular contraction. *Science.* 164:1356–1365.
4. Rayment, I., W. R. Rypniewski, K. Schmidt-Base, R. Smith, D. R. Tomchick, et al. 1993. Three-dimensional structure of myosin subfragment-1: a molecular motor. *Science.* 261:50–58.
5. Schroder, R. R., D. J. Manstein, W. Jahn, H. Holden, I. Rayment, et al. 1993. Three-dimensional atomic model of F-actin decorated with *Dictyostelium* myosin S1. *Nature.* 364:171–174.
6. Holmes, K. C., I. Angert, F. J. Kull, W. Jahn, and R. R. Schroder. 2003. Electron cryo-microscopy shows how strong binding of myosin to actin releases nucleotide. *Nature.* 425:423–427.
7. Rayment, I., H. M. Holden, M. Whittaker, C. B. Yohn, M. Lorenz, et al. 1993. Structure of the actin-myosin complex and its implications for muscle contraction. *Science.* 261:58–65.
8. Holmes, K. C. 1997. The swinging lever-arm hypothesis of muscle contraction. *Curr. Biol.* 7:R112–R118.
9. Geeves, M. A., and K. C. Holmes. 1999. Structural mechanism of muscle contraction. *Annu. Rev. Biochem.* 68:687–728.
10. Huxley, H. E., and W. Brown. 1967. The low-angle x-ray diagram of vertebrate striated muscle and its behaviour during contraction and rigor. *J. Mol. Biol.* 30:383–434.
11. Haselgrove, J. C. 1975. X-ray evidence for conformational changes in the myosin filaments of vertebrate striated muscle. *J. Mol. Biol.* 92:113–143.
12. Huxley, H. E., A. R. Faruqi, M. Kress, J. Bordas, and M. H. J. Koch. 1982. Time-resolved X-ray diffraction studies of the myosin layer-line reflections during muscle contraction. *J. Mol. Biol.* 158:637–684.
13. Bordas, J., G. P. Diakun, F. G. Diaz, J. E. Harries, R. A. Lewis, et al. 1993. Two-dimensional time-resolved x-ray diffraction studies of live isometrically contracting frog sartorius muscle. *J. Muscle Res. Cell Motil.* 14:311–324.
14. Brenner, B., and L. C. Yu. 1993. Structural changes in the actomyosin cross-bridges associated with force generation. *Proc. Natl. Acad. Sci. USA.* 90:5252–5256.

15. Dobbie, I., M. Linari, G. Piazzesi, M. Reconditi, N. Koubassova, et al. 1998. Elastic bending and active tilting of myosin heads during muscle contraction. *Nature*. 396:383–387.

16. Kraft, T., T. Mattei, A. Radocaj, B. Piep, C. Nocula, et al. 2002. Structural features of cross-bridges in isometrically contracting skeletal muscle. *Biophys. J.* 82:2536–2547.

17. Ferenczi, M. A., S. Y. Bershitsky, N. Koubassova, V. Siththanandan, W. I. Helsby, et al. 2005. The ''roll and lock'' mechanism of force generation in muscle. *Structure*. 13:131–141.

18. Huxley, H., M. Reconditi, A. Stewart, and T. Irving. 2001. 2006. X-ray interference studies of crossbridge action in muscle contraction: evidence from quick releases. *J. Mol. Biol.* 363:743–761.

19. Huxley, A. F., and R. M. Simmons. 1971. Proposed mechanism of force generation in striated muscle. *Nature*. 233:533–538.

20. Brenner, B. 1991. Rapid dissociation and reassociation of actomyosin cross-bridges during force generation: a newly observed facet of cross-bridge action in muscle. *Proc. Natl. Acad. Sci. USA*. 88:10490–10494.

21. Brenner, B., J. M. Chalovich, and L. C. Yu. 1995. Distinct molecular processes associated with isometric force generation and rapid tension recovery after quick release. *Biophys. J.* 68:106S–111S.

22. Fortune, N. S., M. A. Geeves, and K. W. Ranatunga. 1991. Tension responses to rapid pressure release in glycerinated rabbit muscle fibers. *Proc. Natl. Acad. Sci. USA*. 88:7323–7327.

23. Kawai, M., and H. R. Halvorson. 1991. Two step mechanism of phosphate release and the mechanism of force generation in chemically skinned fibers of rabbit psoas muscle. *Biophys. J.* 59:329–342.

24. Dantzig, J. A., Y. E. Goldman, N. C. Millar, J. Lacktis, and E. Homsher. 1992. Reversal of the cross-bridge force-generating transition by photogeneration of phosphate in rabbit psoas muscle fibres. *J. Physiol.* 451:247–278.

25. Ranatunga, K. W. 1999. Effects of inorganic phosphate on endothermic force generation in muscle. *Proc. Biol. Sci.* 266:1381–1385.

26. Chen, Y. D., and B. Brenner. 1993. On the regeneration of the actin-myosin power stroke in contracting muscle. *Proc. Natl. Acad. Sci. USA*. 90:5148–5152.

27. Ford, L. E., A. F. Huxley, and R. M. Simmons. 1977. Tension responses to sudden length change in stimulated frog muscle fibres near slack length. *J. Physiol.* 269:441–515.

28. Radocaj, A., T. Weiss, W. Helsby, T. Kraft, and B. Brenner. 2007. 2D-x-ray diffraction study of structural properties of force generating cross-bridges. *Biophys. J.* 92:L180a. (Abstr.)

29. Brenner, B. 1983. Technique for stabilizing the striation pattern in maximally calcium-activated skinned rabbit psoas fibers. *Biophys. J.* 41:99–102.

30. Yu, L. C., and B. Brenner. 1989. Structures of actomyosin cross-bridges in relaxed and rigor muscle fibers. *Biophys. J.* 55:441–453.

31. Kraft, T., M. Messerli, B. Rothen-Rutishauser, J. C. Perriard, T. Wallimann, et al. 1995. Equilibration and exchange of fluorescently labeled molecules in skinned skeletal muscle fibers visualized by confocal microscopy. *Biophys. J.* 69:1246–1258.

32. Kraft, T., S. Xu, B. Brenner, and L. C. Yu. 1999. The effect of thin filament activation on the attachment of weak binding cross-bridges: a two-dimensional x-ray diffraction study on single muscle fibers. *Biophys. J.* 76:1494–1513.

33. Kraft, T., L. C. Yu, H. J. Kuhn, and B. Brenner. 1992. Effect of Ca^{2+} on weak cross-bridge interaction with actin in the presence of adenosine 5′-[gamma-thio]triphosphate. *Proc. Natl. Acad. Sci. USA*. 89:11362–11366.

34. Pate, E., G. J. Wilson, M. Bhimani, and R. Cooke. 1994. Temperature dependence of the inhibitory effects of orthovanadate on shortening velocity in fast skeletal muscle. *Biophys. J.* 66:1554–1562.

35. Zhao, Y., and M. Kawai. 1994. Kinetic and thermodynamic studies of the cross-bridge cycle in rabbit psoas muscle fibers. *Biophys. J.* 67:1655–1668.

36. Davis, J. S., and M. E. Rodgers. 1995. Force generation and temperature-jump and length-jump tension transients in muscle fibers. *Biophys. J.* 68:2032–2040.

37. Ranatunga, K. W. 1996. Endothermic force generation in fast and slow mammalian (rabbit) muscle fibers. *Biophys. J.* 71:1905–1913.

38. Godt, R. E., and D. W. Maughan. 1988. On the composition of the cytosol of relaxed skeletal muscle of the frog. *Am. J. Physiol.* 254:C591–C604.

39. Kraft, T., E. Mahlmann, T. Mattei, and B. Brenner. 2005. Initiation of the power stroke in muscle: insights from the phosphate analog AlF4. *Proc. Natl. Acad. Sci. USA*. 102:13861–13866.

40. Lewis, R. A., C. J. Hall, W. Helsby, A. Jones, B. Parker, et al. 1995. 10-MHz photon counting detector system for time-resolved x-ray diffraction. *Proc. SPIE. 290–300*.

41. Lewis, R. A., A. Berry, C. J. Hall, W. I. Helsby, and B. T. Parker. 1999. RAPID detector system: first user data. *Proc. SPIE. 97–102*.

42. Xu, S., S. Malinchik, D. Gilroy, T. Kraft, B. Brenner, et al. 1997. X-ray diffraction studies of cross-bridges weakly bound to actin in relaxed skinned fibers of rabbit psoas muscle. *Biophys. J.* 73: 2292–2303.

43. Bordas, J., A. Svensson, M. Rothery, J. Lowy, G. P. Diakun, et al. 1999. Extensibility and symmetry of actin filaments in contracting muscles. *Biophys. J.* 77:3197–3207.

44. Kress, M., H. E. Huxley, A. R. Faruqi, and J. Hendrix. 1986. Structural changes during activation of frog muscle studied by time-resolved x-ray diffraction. *J. Mol. Biol.* 188:325–342.

45. Goody, R. S., and F. Eckstein. 1971. Thiophosphate analogs of nucleoside di- and triphosphates. *J. Am. Chem. Soc.* 93:6252–6257.

46. Bagshaw, C. R., J. F. Eccleston, D. R. Trentham, D. W. Yates, and R. S. Goody. 1973. Transient kinetic studies of the Mg^{++}-dependent ATPase of Myosin and its proteolytic subfragments. *Cold Spring Harbor Symp. Quant. Biol.* 37:127–135.

47. Koubassova, N. A., and A. K. Tsaturyan. 2002. Direct modeling of x-ray diffraction pattern from skeletal muscle in rigor. *Biophys. J.* 83:1082–1097.

48. Koubassova, N. A., S. Y. Bershitsky, M. A. Ferenczi, and A. K. Tsaturyan. 2008. Direct modeling of x-ray diffraction pattern from contracting skeletal muscle. *Biophys. J.* 95:2880–2894.

49. Tregear, R. T., M. C. Reedy, Y. E. Goldman, K. A. Taylor, H. Winkler, et al. 2004. Cross-bridge number, position, and angle in target zones of cryofixed isometrically active insect flight muscle. *Biophys. J.* 86:3009–3019.

50. Brenner, B., L. C. Yu, and R. J. Podolsky. 1984. X-ray diffraction evidence for cross-bridge formation in relaxed muscle fibers at various ionic strengths. *Biophys. J.* 46:299–306.

51. Brenner, B., and L. C. Yu. 1985. Equatorial x-ray diffraction from single skinned rabbit psoas fibers at various degrees of activation. Changes in intensities and lattice spacing. *Biophys. J.* 48:829–834.

52. Vainstein, B. K. 1966. Diffraction of X-Rays by Chain Molecules. Elsevier Publishing, Amsterdam.

53. Brenner, B. 1998. Muscle mechanics II: skinned muscle fibres. *In* Current Methods in Muscle Physiology. Advantages, Problems and Limitations. H. Sugi, editor. Oxford University Press, Oxford 33–69.

54. Brenner, B. 1985. Sarcomeric domain organization within single skinned rabbit psoas fibers and its effects on laser light diffraction patterns. *Biophys. J.* 48:967–982.

55. Rudel, R., and F. Zite-Ferenczy. 1979. Interpretation of light diffraction by cross-striated muscle as Bragg reflexion of light by the lattice of contractile proteins. *J. Physiol.* 290:317–330.

56. Piazzesi, G., M. Reconditi, M. Linari, L. Lucii, P. Bianco, et al. 2007. Skeletal muscle performance determined by modulation of number of myosin motors rather than motor force or stroke size. *Cell.* 131:784–795.

57. Ford, L. E., A. F. Huxley, and R. M. Simmons. 1985. Tension transients during steady shortening of frog muscle fibres. *J. Physiol.* 361: 131–150.

58. Stehle, R., and B. Brenner. 2000. Cross-bridge attachment during high-speed active shortening of skinned fibers of the rabbit psoas muscle: implications for cross-bridge action during maximum velocity of filament sliding. *Biophys. J.* 78:1458–1473.

59. Roots, H., G. W. Offer, and K. W. Ranatunga. 2004. 2007. Comparison of the tension responses to ramp shortening and lengthening in intact mammalian muscle fibres: crossbridge and non-crossbridge contributions. *J. Muscle Res. Cell Motil.* 28:123–139.

60. Pinniger, G. J., K. W. Ranatunga, and G. W. Offer. 2006. Crossbridge and non-crossbridge contributions to tension in lengthening rat muscle: force-induced reversal of the power stroke. *J. Physiol.* 573:627–643.

61. Yagi, N., H. Iwamoto, J. Wakayama, and K. Inoue. 2005. Structural changes of actin-bound myosin heads after a quick length change in frog skeletal muscle. *Biophys J.* 89:1150–1164.